Solid-State Electronics Vol. 32, No. 2, pp. 149–157, 1989
Printed in Great Britain.

0038-1101/89 $3.00 + 0.00

SIMULATION OF THE AMORPHOUS SILICON STATIC INDUCTION TRANSISTOR

M. KEMP, M. MEUNIER† and C. G. TANNOUS

Groupe des Couches Minces and Département de génie physique, Ecole Polytechnique, C.P. 6079, Succursale "A" Montréal, Qc Canada H3C 3A7

(*Received* 7 *May* 1988; *in revised form* 29 *July* 1988)

Abstract—The I–V characteristics of the hydrogenated amorphous silicon Static Induction Transistor are obtained by performing a simulation in two dimensions considering electrons and holes together for the first time. The results show that the device has basically four modes of operation that we identify and interpret physically: saturation, channel opening, ohmic and drain current inversion. The study of the influence of the electron concentration at the ohmic contacts, the channel width and the deep level density of states on the switching properties of the device is undertaken. Besides, we show that the on-current is controlled by the electron concentration at the ohmic contacts whereas the off-current is controlled by the electron concentration at the Schottky contact. Finally, we show that the turn-off voltage increases when the channel width or the deep level density of states increase.

NOTATION

A	transverse surface of a single channel device
d	distance between two terminals in the 1-D diode model
D_n	electron diffusion constant
D_p	hole diffusion constant
e_n	emission rate for electrons
e_p	emission rate for holes
E_c	conduction band edge energy
E_f	Fermi level
E_{fn}	electron quasi-Fermi level
E_g	energy gap
E_i	intrinsic energy level
E_t^*	characteristic energy
E_v	valence band edge energy
f	probability of occupation of trap states
g_{Ai}	type i acceptor density of states
g_{Di}	type i donor density of states
I_D	drain current
I_G	gate current
I_{off}	off-current
I_{on}	on-current
I_S	source current
$\mathbf{J}_n$	electron current density
$\mathbf{J}_p$	hole current density
kT	Boltzmann constant times temperature T
L	gate to gate distance
n	electron concentration
n_i	intrinsic concentration
n_o	electron concentration at the ohmic contacts
$n_{Schottky}$	electron concentration at the Schottky contact
n_t	trapped electron concentration
N	number of channels
N_{ohmic}	dopant concentration at the ohmic contacts
p	hole concentration
p_o	hole concentration at the ohmic contacts
$p_{Schottky}$	hole concentration at the Schottky contact
p_t	trapped hole concentration
q	electron charge
R	recombination rate
v_{th}	thermal velocity
V_{ds}	drain-source voltage
V_{gs}	gate-source voltage
V_{off}	turn-off voltage
x_0	length of the depleted region in the 1-D diode model
ϵ	a-Si:H permittivity
ϵ_0	free space permittivity
μ_n	electron mobility
μ_p	hole mobility
σ_n	electron capture cross-section
σ_p	hole capture cross-section
σ_{Adn}	electron capture cross-section of acceptor-like deep states
σ_{Adp}	hole capture cross-section of acceptor-like deep states
σ_{Atn}	electron capture cross-section of acceptor-like tail states
σ_{Atp}	hole capture cross-section of acceptor-like tail states
σ_{Ddn}	electron capture cross-section of donor-like deep states
σ_{Ddp}	hole capture cross-section of donor-like deep states
σ_{Dtn}	electron capture cross-section of donor-like tail states
σ_{Dtp}	hole capture cross-section of donor-like tail states
ϕ_B	contact potential
ψ	electrostatic potential
ψ_0	ohmic contact electrostatic potential
$\psi_{Schottky}$	Schottky contact electrostatic potential

†To whom correspondence should be addressed.

1. INTRODUCTION

The low temperature and large area deposition properties of hydrogenated amorphous silicon (a-Si:H) has stimulated research as to the capability of such a semiconductor to efficiently enter in the fabrication of switching elements for large area liquid-crystal displays. The low drift mobility of this material and problems attributed to the presence of traps at the insulator/a-Si:H interface in MISFET type structures[1] have led Ueda *et al.* [2] to propose the use of the Static Induction Transistor (SIT) geometry for this application. Performing a 1-D analysis of the

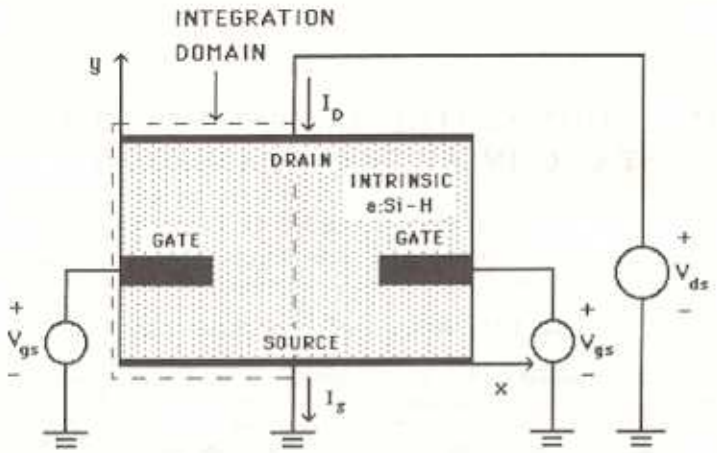

Fig. 1. Schematic representation of the a-Si:H SIT. The dashed line is the mirror symmetry axis. Only the left part of the figure is needed in the simulation.

operation of the device, Ueda *et al.*[2] showed that a-Si:H may efficiently be used for the realization of such switches.

Basing our analysis on a 2-D numerical simulation which takes realistically account of most a-Si:H parameters, we aim in this work for a deeper understanding of the d.c. operation of the a-Si:H SIT with the goal of identifying the most significant switching design parameters. This analysis takes into account both types of carriers, reflecting the crucial dependance minority carriers have on the occupation of the traps. In the next section, we present the model and the calculation techniques on which the analysis is based. We show in Section 3 that the transfer characteristics are composed of four modes of operation. We also show that although the global behavior of the amorphous SIT bears a resemblance with its crystalline homonym, the underlying mechanisms are radically different. Section 4 deals with the influence of design parameters on the switching properties. We identify the physical factors influencing these properties and give some guidelines for the optimum design of the device.

2. THEORETICAL ANALYSIS

2.1. Model

The Static Induction Transistor we consider in these simulations is composed of the periodic repetition of N of the cell structures shown in Fig. 1. In this figure, both the source and drain are ohmic contacts, the gate is a Schottky contact and the bulk of the device is filled with intrinsic a-Si:H. Using translational symmetry from cell to cell, mirror symmetry about the center line in the channel and the fact the length of the gate is three orders of magnitude larger than the two other linear dimensions, only half of a 2-D cell is needed in the simulation.

The basic equations for the description of the static operation of the device are:

$$\nabla^2\psi = \frac{-q}{\epsilon}(p - n + p_t - n_t) \tag{1}$$

$$\operatorname{div} \mathbf{J}_n = qR, \tag{2}$$

$$\operatorname{div} \mathbf{J}_p = -qR, \tag{3}$$

where p_t and n_t are the trapped hole and electron concentrations. The electron and hole current densities $\mathbf{J}_n$ and $\mathbf{J}_p$ are given by:

$$\mathbf{J}_n = qD_n\left(\nabla n - \frac{q}{kT} n \nabla\psi\right), \tag{4}$$

$$\mathbf{J}_p = -qD_p\left(\nabla p + \frac{q}{kT} p \nabla\psi\right), \tag{5}$$

where the Einstein relations valid for non-degenerate semiconductors have been used. All scalar and vector differential operators are used in their 2-D form.

Equations (1)–(5) are subject to two boundary conditions. At the ohmic contacts, conditions of thermal equilibrium and space charge neutrality are assumed, that is:

$$p_\circ n_\circ = n_i^2 \tag{6}$$

$$p_t(n_\circ, p_\circ) - n_t(n_\circ, p_\circ) + p_\circ - n_\circ + N_{\text{ohmic}} = 0 \tag{7}$$

$$\psi_\circ = V_{\text{applied}} + \frac{kT}{q}\log\frac{n_\circ}{n_i} \tag{8}$$

where $n_\circ$ and $p_\circ$, the electron and hole concentrations at the ohmic contacts are solution to the coupled non-linear equations (6)–(7) and where N_{ohmic} is the activated dopant concentration at the ohmic contacts. In this paper, we assume that N_{ohmic} is identical at both contacts. At the Schottky contact, we assume also thermal equilibrium which leads to[3]:

$$n_{\text{Schottky}} = n_i \exp\left[\frac{E_g/2 - q\phi_B}{kT}\right] \tag{9}$$

$$p_{\text{Schottky}} = n_i^2/n_{\text{Schottky}} \tag{10}$$

$$\psi_{\text{Schottky}} = V_{\text{applied}} + \frac{E_g}{2q} - \phi_B. \quad (11)$$

On all the remaining boundaries, the mirror symmetry enforces:

$$\frac{\partial \psi}{\partial x} = \frac{\partial n}{\partial x} = \frac{\partial p}{\partial x} = 0, \quad (12)$$

where the coordinate convention is indicated in Fig. 1.

Hydrogenated amorphous silicon is characterized by a continuous distribution of localized states. We assume the density of states (DOS) to be composed of four bands: a donor-like valence band tail, an acceptor-like conduction band tail and two deep levels bands, one acceptor-like the other donor-like. Using a model intermediate between the one used by Sakata and Hayashi[4] and the other by Müller *et al.*[5], we describe the DOS by:

$$g(E) = g_{At}(E) + g_{Dt}(E) + g_{Ad}(E) + g_{Dd}(E) \quad (13)$$

$$g_{At}(E) = g_t \exp\left[\frac{E - E_t}{W_C}\right] \quad (14)$$

$$g_{Dt}(E) = g_t \exp\left[\frac{E_t - E}{W_V}\right], \quad (15)$$

$$g_{Ad}(E) = g_D \exp\left[-\frac{1}{2}\left[\frac{E - E_A}{W_D}\right]^2\right], \quad (16)$$

$$g_{Dd}(E) = g_D \exp\left[-\frac{1}{2}\left[\frac{E - E_D}{W_D}\right]^2\right], \quad (17)$$

where the subscripts A, D, t, d stand for acceptor, donor, tail and deep states respectively and where the values of the DOS parameters E_t, E_A, E_D, W_C, W_V and W_D are given in Table 1.

We treat the occupation of the mobility gap states according to the analysis developed by Simmons and Taylor[6]. We neglect the correlation between the deep levels by doing so. In the steady-state, the probability of occupation of a trap level at energy E is given by:

$$f(E, n, p) = \frac{v_{th}\sigma_n n + e_p}{v_{th}(\sigma_n n + \sigma_p p) + (e_n + e_p)}, \quad (18)$$

with $e_n = v_{th}\sigma_n n_1 \exp[(E - E_t)/(kT)]$ and $e_p = v_{th}\sigma_p n_1 \exp[(E_t - E)/(kT)]$. Following Sakata and Hayashi[4] we further assume that the capture cross-sections are both constant for all energies in a given band.

The densities of trapped carriers are given by:

$$n_t(n, p) = \sum_i \int_{E_v}^{E_c} dE\, g_{Ai}(E) f_{Ai}(E, n, p), \quad (19)$$

$$p_t(n, p) = \sum_i \int_{E_v}^{E_c} dE\, g_{Di}(E)[1 - f_{Di}(E, n, p)], \quad (20)$$

where the summation runs over all acceptor band types for n_t and over all donor bands for p_t (i stands for t and d representing tail and deep states respectively and $f_{Ai}(E, n, p)$ [respectively $f_{Di}(E, n, p)$] is obtained from eqn (18) through the replacement of σ_n and σ_p by σ_{Ain} and σ_{Aip} [respectively σ_{Din} and σ_{Dip}]). The recombination rate is given by:

$$R(n, p) = \sum_l \int_{E_v}^{E_c} \times dE \frac{[v_{th}^2 \sigma_{ln}\sigma_{lp} np - e_n e_p]}{v_{th}(\sigma_{ln} n + \sigma_{lp} p) + (e_n + e_p)} g_l(E) \quad (21)$$

where the summation runs over all types of donor and acceptor bands (l stands for *At*, *Ad*, *Dt* and *Dd*).

Table 1. Parameters used in the simulations

ϵ	$11.7\,\epsilon_0$
μ_n	$10\ \text{cm}^2\,\text{V}^{-1}\,\text{s}^{-1}$
μ_p	$0.1\ \text{cm}^2\,\text{V}^{-1}\,\text{s}^{-1}$
n_i	$5 \times 10^7\ \text{cm}^{-3}$
E_g	1.7 eV
E_t	0 eV
E_t	0.1 eV
n_0	$10^{11}\ \text{cm}^{-3}$
ϕ_B	1 V
g_t	$10^{14}\ \text{cm}^{-3}\,\text{eV}^{-1}$
g_D	$10^{16}\ \text{cm}^{-3}\,\text{eV}^{-1}$
E_f	0.1 eV
W_V	0.0616 eV
W_C	0.0485 eV
E_D	−0.15 eV
E_A	0.35 eV
W_D	0.15 eV
v_{th}	$10^7\ \text{cm s}^{-1}$
$\sigma_{Dtn} = \sigma_{Atp}$	$10^{-15}\ \text{cm}^2$
$\sigma_{Atn} = \sigma_{Dtp}$	$10^{-14}\ \text{cm}^2$
$\sigma_{Ddn} = \sigma_{Adp}$	$10^{-16}\ \text{cm}^2$
$\sigma_{Adn} = \sigma_{Ddp}$	$10^{-18}\ \text{cm}^2$
Drain to source spacing	3.3 μm
Source to gate spacing	1.0 μm
Gate to drain spacing	2.0 μm
Gate width	2.0 μm
Gate thickness	0.3 μm
Center of gate to center of gate spacing	4.0 μm
Number of cells	100

Table 1 lists all relevant parameters used in the simulations are presented in Table 1. Let us point out that electron and hole mobilities are both assumed constant.

2.2. Calculation techniques

Equations (1)–(5) together with the models for n_t, p_t and R form a set of coupled non-linear partial differential equations, to be solved on the 2-D geometry of Fig. 1 with the boundary conditions given by eqns (6)–(12). The numerical techniques we use to solve these equations are based on finite differences methods. Since the coupling between the dynamics of trapped carriers and the free ones is to be accounted for, we use a linear version of the adapted Gummel method that we developed in detail elsewhere[8, 9]. The continuity equations are both discretized by the Scharfetter–Gummel[10] method and the evaluation of the recombination rate is performed at the beginning of each iteration. The iteration procedure is stopped when either the maximum relative correction is less than 10^{-10} or when the number of iterations exceeds 20. The simulations are performed on a 21×31 grid. We checked that the error on the

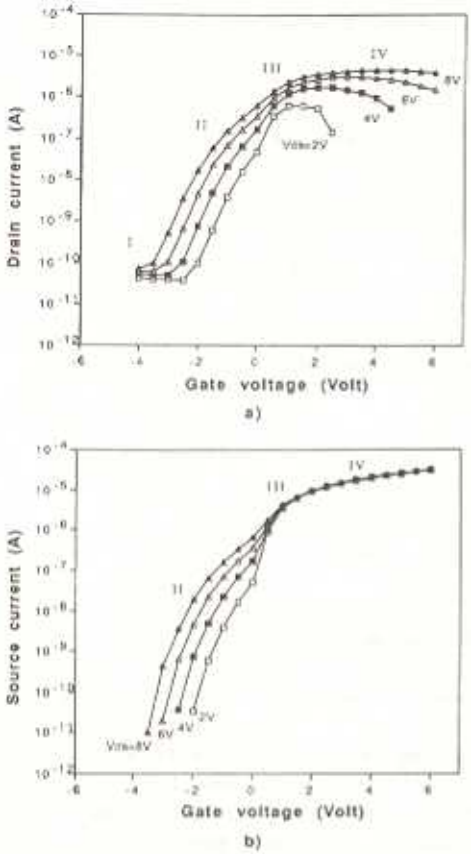

Fig. 2. Transfer characteristics of the a-Si:H SIT: (a) drain characteristic; (b) source characteristic. The four operation modes are identified with roman numerals.

current involved with such a small grid is less than 1% by going to larger sizes.

3. ANALYSIS OF THE I–V RESULTS

The SIT with the parameters of Section 2 is simulated with the goal of extracting the I–V characteristics. Figure 2 shows the transfer characteristics of the drain and source current I_D and I_S with the drain biased at 2, 4, 6 and 8 V. For means of comparison with Ref.[2], the current in this and other figures is N times the single channel device current, where the number of channels N is taken as 100 except if explicitly stated. There exist four modes of operation which we called saturation (I), channel opening (II), ohmic regime (III) and drain current inversion (IV). We wish to show that this nomenclature is indeed the correct one and do so by first identifying the physical mechanisms underlying the four modes and second, by supporting the analysis with a 1-D approach allowing us to recover independently our main results. Before we proceed, we first analyse the gate leakage current since most of the discussion that follows relies on it.

3.1. Gate leakage current

The study of the gate leakage current is performed by grounding both the source and drain and by

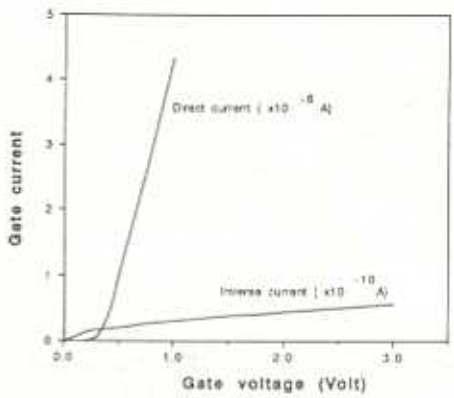

Fig. 3. I_G–V_{gs} characteristic of the device when source and drain are both grounded.

applying a bias on the gate. To simplify the analysis, the geometry is taken with the gate halfway between the ohmic contacts. From Fig. 3 where the gate current I_G is plotted as a function of V_{gs}, we note that the characteristic has a saturating behavior when $V_{gs} < 0$ and an exponential one at low positive bias followed by an ohmic regime at higher voltages. Thus the device has a diode-like operation mode, which is expected from its geometry as we show below.

The calculated reverse bias results are supported by a 1-D analysis based on the diffusion model and on an extension of a model presented first by Suzuki *et al.*[7]. The diffusion model predicts for 1-D diode the relation[11]:

$$I_G = NAn_i kT\mu_n \left(\exp\frac{qV}{kT} - 1\right) \Big/ \int_0^d \mathrm{d}x \exp\left(\frac{-q\psi(x)}{kT}\right), \tag{22}$$

where d is the length of the diode (1.5 μm), A the transverse surface of a single diode and N the number of diodes in parallel. In the work of Suzuki *et al.*[7], the potential distribution $\psi(x)$ for an infinitely long a-Si:H Schottky diode in the reverse mode is obtained. The extension to a finite length device is presented in Appendix A. These models can be used to predict the behavior of the leakage current in the SIT because the semiconductor variables are essentially 1-D in the regions between the source and gate and between the drain and gate; besides, the effect of the channel on I_G is negligible when the drain is grounded. The predicted and calculated values of the gate current in the reverse mode are presented in Fig. 4. The agreement between the two curves is quite good since no parameter fitting procedure was attempted.

As the applied bias is increased to positive values, the depletion region shrinks leaving a bulk electron concentration equal to its ohmic contact value. Therefore the conduction is drift dominated and should be ohmic since the electron concentration is constant. The electron current density equation predicts in that case that the slope of the I–V curve is

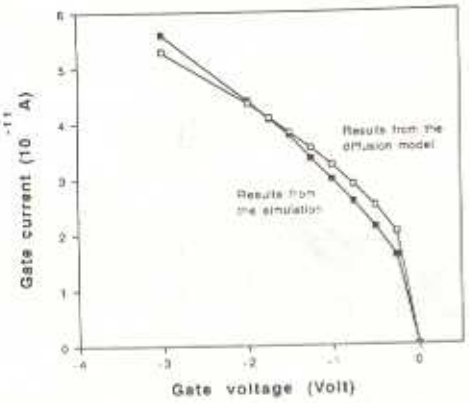

Fig. 4. Comparison of the numerically obtained results with the analytical predictions of the diffusion model for the leakage current characteristic of the device in the reverse mode.

given by:

$$\left(\frac{\Delta I}{\Delta V}\right)=\frac{NA}{d}q\mu_n n_0 \qquad (23)$$

Using the values given in Table 1, the predicted slope is 4.3×10^{-6} mho while the one obtained from the simulation is 6.8×10^{-6} mho. The slight difference between these values is attributed to the bulk electron concentration which is not rigorously equal to its contact value.

3.2. Analysis of the I–V characteristics

It is generally admitted[12–14] that the crystalline SIT is a drift dominated unipolar majority carrier device when $V_{gs}<0$. This statement is also correct for the amorphous SIT and is supported by the following facts: 1. In undoped a-Si:H, the Fermi level lies above midgap, leading to an equilibrium electron concentration three orders of magnitude larger than the hole concentration; 2. the electron mobility is larger than the hole mobility; 3. the electron concentration in the effective channel is almost constant and the drift component of the total channel current is more important than the diffusion one. With all these facts, we conclude that the channel current is essentially a drift electron current and should be proportional to the channel electron concentration.

The geometry of the amorphous SIT is slightly different from the one used with crystalline materials, in that the gate is totally embedded in the bulk of the device (to that respect, our geometry is more closely related to the PBT[3]). The interpretation of the I–V characteristics is simplified if one realises that the drain current is given by two contributions: (i) a channel current from drain to source, the magnitude of which is mediated via the effect of the gate on the channel electron concentration, and (ii) a leakage current from gate to drain whose diode-like behavior was studied in Section 3.1. Similar remarks apply at the source. In the four following subsections, we show that it is the relative importance of each of these components that gives its four mode structures to the I–V characteristics. For the analysis, we have chosen $V_{ds}=4$ V and V_{gs} going from -4 to 4 V.

3.2.1. Mode I: saturation. The calculated electron concentration distribution at $V_{ds}=4$ V and $V_{gs}=-3$ V is shown in Fig. 5(a). It shows clearly that the entire bulk of the device is depleted meaning that both the channel and the leakage currents from gate to source and from gate to drain are small. While the channel current decreases as V_{gs} takes more negative values, the diffusion model of Section 3.1 shows that any of the leakage currents increase with it. Thus, as V_{gs} is decreased (goes more negative) below a certain threshold V_{off}, the behavior of I_D and I_S is taken over by the leakage currents.

3.2.2. Mode II: channel opening. As the gate voltage is increased (less negative) above V_{off}, the electron concentration in the channel builds up as is shown in Fig. 5(b), giving rise to the increase in I_D and I_S. Note that the leakage currents have no effect whatsoever on I_D and I_S since their values are small and almost independent of V_{gs}.

The behavior of the current as the channel opens up can be accounted for by a 1-D model similar to the one proposed by Ueda *et al.*[2] describing the evolution of the channel current in the a-Si:H SIT as a function of V_{gs}. The modifications we bring to this model account to a certain extent for the spatial variation of the electron quasi-Fermi potential in the channel by modelling it with a parabolic function, and the spatial variation of the amplification factor through the use of a linear function of position. Figure 6 shows that the analytically predicted and numerically calculated channel current are in good agreement since the values predicted were obtained with no best-fit parameter calculation. Pushing the model further, the operation of the device in the channel opening mode is described in the following: first, there is an exponential build-up of the electron concentration at the center of the channel. This build-up is effective until n reaches the concentration at the ohmic contacts which corresponds to its maximum permitted value. Once this condition is fulfilled, the rest of the channel starts getting filled until the local concentration reaches the same value and this leads to the slower increases of I as V_{gs} approaches 0 V.

A similar behavior was observed in the crystalline SIT[12, 13] where the exponential regime was attributed to a linear lowering of the barrier height by the gate voltage. The departure from the exponential increase in the high current range was attributed to a space-charge compensation by the channel electron, leading to a self-adjusted value of the barrier height[13]. An identical behavior of the barrier height takes place in the amorphous SIT, however the physical mechanisms responsible for its variation are of a completely different nature. In amorphous semiconductors, the space-charge is equal to the trapped charge, which in turn is coupled in a complex fashion

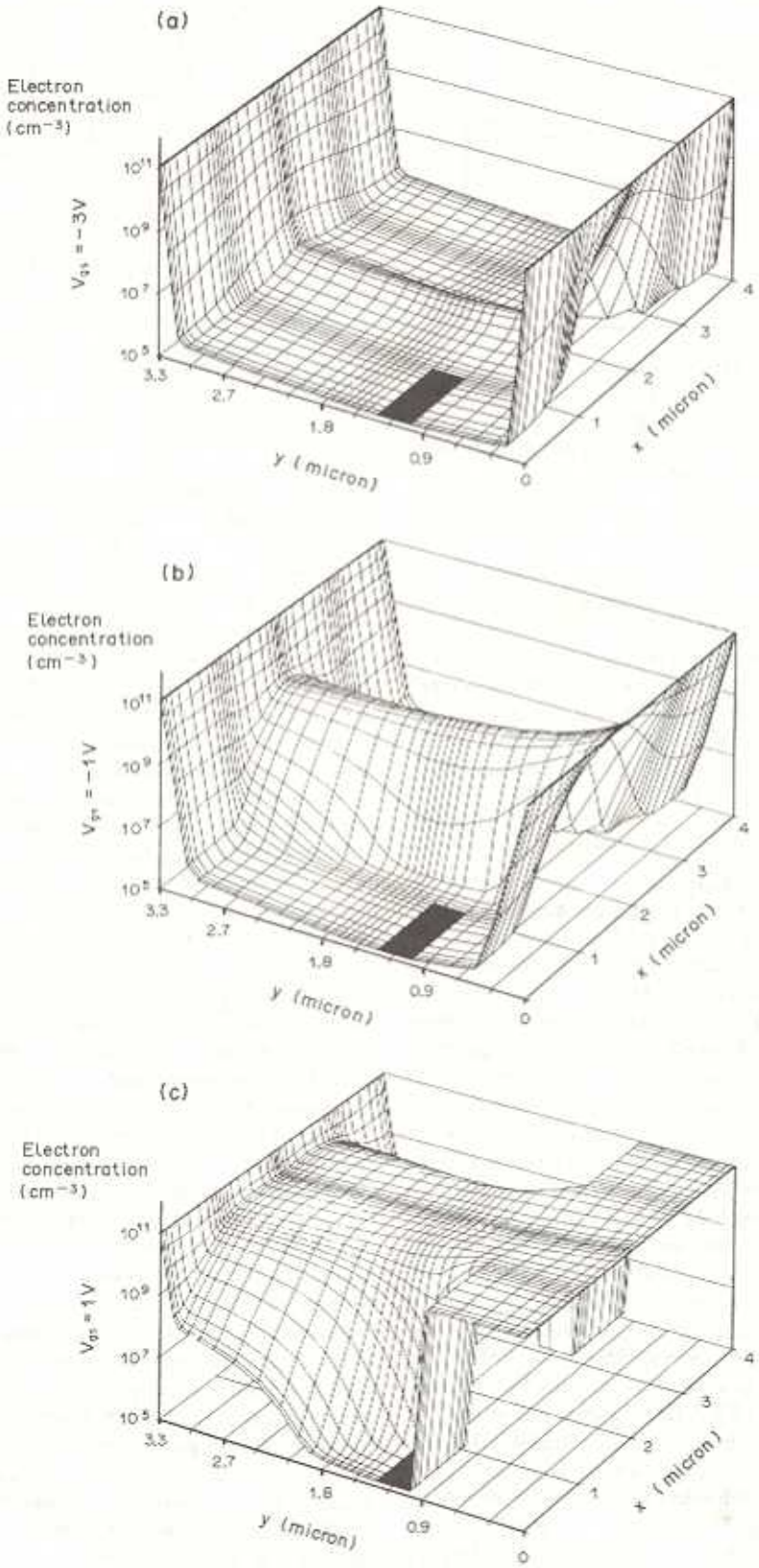

Fig. 5. Distribution of the electron concentration in the device for various values of V_{gs}: (a) $V_{gs} = -3$ V; (b) $V_{gs} = -1$ V; (c) $V_{gs} = 1$ V. These results are obtained for $V_{ds} = 4$ V.

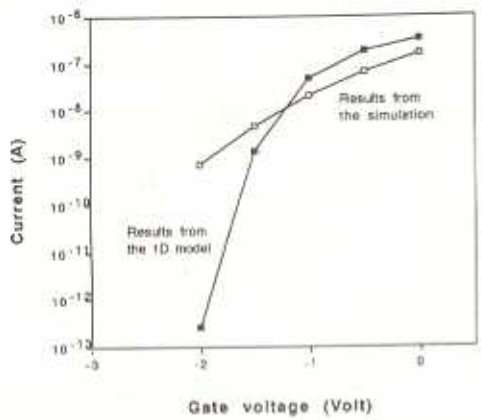

Fig. 6. Comparison of the numerically calculated results with the analytical predictions of the Ueda *et al.* model for the channel current in the channel opening mode. Both curves are obtained with $V_{ds} = 4$ V.

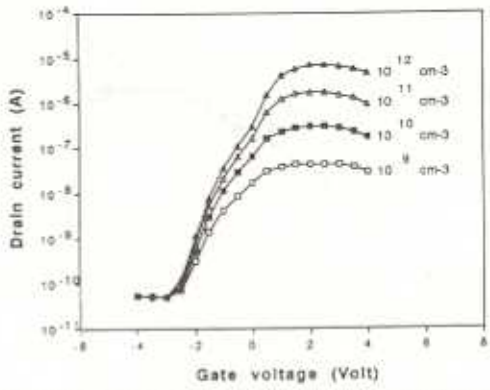

Fig. 7. Effect of varying the electron concentration at the ohmic contacts. These results are obtained with $V_{ds} = 4$ V.

to n and p via the occupation function (18). The apparent complexity of this relation hides two important facts, first that at low n and p the trapped charge is constant, and second that any increase in n diminishes substantially the trapped charge. Consequently, the space-charge behaves as in the crystalline case but the cause of its variation is linked to the non-linearity of the relation between n and the trapped charge. The slower increase of the current as V_{gs} approaches 0 V should not be confused with the space-charge-limited operation that takes place in the crystalline SIT, since the space-charge is always large and never compensated by the electronic charge.

3.2.3. Mode III: ohmic regime. While the leakage currents can be neglected in the channel opening mode, the leakage from gate to source becomes important in the ohmic regime mode because V_{gs} by changing from negative to positive becomes a forward bias acting on the Schottky diode between gate and source. Figure 5(c) shows that the electron concentration is more important in the gate to source region than elsewhere and this explains why the associated leakage current dominates the source current. As discussed in Section 3.1, the observed characteristic is linear because of the ohmic losses.

3.2.4. Mode IV: drain current inversion. As the gate voltage takes on values larger than the drain voltage, the polarity between the gate and drain changes sign and the associated large leakage current overwhelms the channel current at the drain. Because the two contributions are opposite in direction, a reversal in the direction of I_D is expected and is in fact observed. However, because the graphics are on a logarithmic scale, only positive values of I_D are plotted.

4. INFLUENCE ON DESIGN PARAMETERS

We showed in Section 3 that the I–V characteristics of the a-Si:H SIT show four modes of operation. Since the scope of this paper is focused on the understanding of the switching properties of the device, we need concern ourselves only with the first two modes. This is because the leakage currents in the last two modes are no longer a perturbation acting on the system but constitute in fact the most important contributions to I_D and I_S.

The switching parameters we consider here are the off-current I_{off}, the on-current I_{on} and the turn-off voltage V_{off}. We define I_{off} as the drain current when the channel is just depleted, I_{on} as the drain current at $V_{gs} = 0$ V and V_{off} as the absolute value of the gate voltage in correspondence with I_{off}. Note that these parameters depend on V_{ds}: we will consider them for $V_{ds} = 4$ V.

The main parameter that controls I_{off} is the electron concentration at the Schottky contact since n takes on this value everywhere when the channel is depleted. On the other hand, when the channel is populated with carriers, the electron concentration at the ohmic contacts n_o is the one which determines the electron concentration anywhere in the channel, therefore I_{on}. The density of deep levels g_D and the channel width L are the most important parameters in the determination of V_{off}. As a first step toward an improvement of the switching parameters of the device, let us consider the effect n_o, I and g_D have on them.

The I_D–V_{gs} characteristics at $V_{ds} = 4$ V for various values of n_o, L and g_D are shown in Figs 7–9 respectively. Figure 7 shows that an increase in n_o increases I_{on} but leaves I_{off} and V_{off} unchanged. These results are readily understood on the basis of the arguments given above. Figure 8 shows that an increase in L increases V_{off} and has almost no effect on the two other quantities. The last two points are also in agreement with the arguments discussed previously. The first feature is explained as follows. The depleted width is a function of both V_{gs} and g_D. If one considers the device in the saturation regime and increases L while keeping all other parameters constant, the center of the channel is no more depleted and the device undergoes a transition from saturation to the channel opening regime. The complete de-

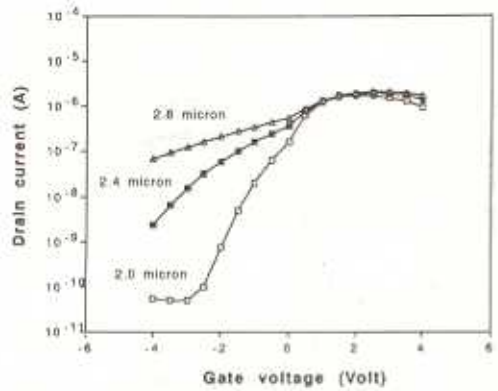

Fig. 8. Effect of varying the channel width. These results are obtained with $V_{ds} = 4$ V.

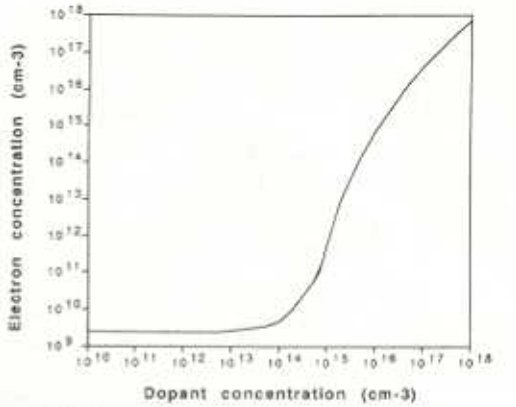

Fig. 10. The electron concentration at the ohmic contacts as a function of the dopant concentration.

pletion of the channel in that case occurs at a lower gate voltage implying that an increase in V_{off} results from an increase in L. Figure 9 shows that an increase in g_D has a similar effect on V_{off}, the reason, this time, being a decrease of the depletion width as g_D increases. This also causes a transition from saturation to the channel opening regime.

These results and the analysis of the device operation give three important guidelines for the optimal design of the a-Si:H SIT. First, I_{on} is controlled in an almost linear way by n_o; second, I_{off} is controlled by $n_{Schottky}$ and thus by ϕ_B; finally, V_{off} increases with the channel width and with density of deep levels. This last point is of paramount importance in the design of LCD displays for it demonstrates that the uniformity of V_{off} is a very sensitive function of the uniformity of the density of deep levels as one goes from one device to another in the transistor matrix.

The practical implementation of an increase in n_o is achieved by the incorporation of a n thin layer at the ohmic contacts. The efficiency of the way the dopant makes n_o increase can be calculated by solving the space charge neutrality eqn (7). Figure 10 shows that n_o is equal to the equilibrium a-Si:H free electron concentration when $N_{ohmic} < 10^{14}$ cm^{-3} and that n_o is a linear function of N_{ohmic} when $N_{ohmic} > 10^{16}$ cm^{-3}. The low concentration result is a consequence of the pinning of the Fermi level E_f by the deep levels density of states, which is operating until N_{ohmic} becomes greater than the number of states per unit volume at E_f in which case the high dopant relation $n_o = N_{ohmic}$ becomes valid. This significant result means that the actual onset of the increase in I_{on} by the dopant occurs when $N_{ohmic} = 10^{14}$ cm^{-3}.

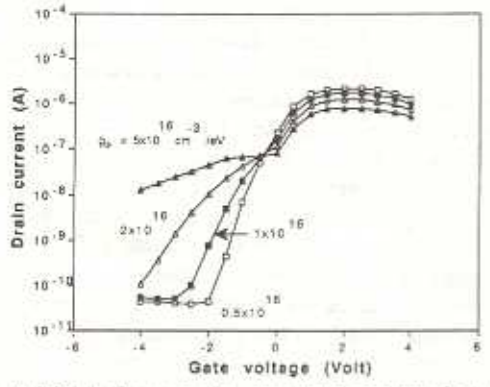

Fig. 9. Effect of varying the deep level density of states. These results are obtained with $V_{ds} = 4$ V.

5. CONCLUSION

The transfer characteristics of the a-Si:H SIT obtained by a spatial finite difference static simulation method in 2-D show clearly four distinct modes of operation. As V_{gs} increases, the device goes through a saturation regime where I_D and I_S are both controlled by the leakage currents originating from the gate, an opening of the channel regime where the leakage currents have no substantial effect, an ohmic regime where I_S is dominated by the leakage currents and a drain current inversion regime where I_D is dominated at its turn by the leakage current. The results obtained by the fully numerical 2-D simulation are reobtained with a simple physical 1-D approach with no adjustable parameters.

The factors having the most significant effect on I_{on}, I_{off} and V_{off} have been identified respectively as the electron concentration at the ohmic contacts, the electron concentration at the Schottky contact and both the channel width and the deep level density of states. We believe that a successful design for the fabrication of a a-Si:H SIT has to build some of its rules on the results we obtained with the 2-D simulation and the simple 1-D analysis.

Acknowledgements—We thank FCAR of Québec and NSERC of Canada for their financial assistance. Discussions with G. W. Harling and G. Perluzzo are gratefully acknowledged.

REFERENCES

1. F. Okumura, S. Kaneko and H. Uchida, *15th Conf. Solid State Devices and Materials*, Extended Abstract p. 201 (1983).

2. M. Ueda, M. Hirose and Y. Osaka, *Jap. J. appl. Phys.* **24,** 467 (1985).
3. C. O. Bozler and G. D. Alley, *IEEE Trans. Electron Dev.* **ED-27,** 1128 (1980).
4. I. Sakata and Y. Hayashi, *Appl. Phys. A* **37,** 153 (1985).
5. G. Müller, H. Mannsperger and S. Kalbitzer, *Phil. Mag.* **55B,** 257 (1986).
6. J. G. Simmons and G. W. Taylor, *Phys. Rev. B* **4,** 502 (1971).
7. T. Suzuki, Y. Osaka and M. Hirose, *Jap. J. appl. Phys.* **22,** 785 (1983).
8. M. Kemp, C. G. Tannous and M. Meunier, *IEEE Trans. Electron Dev.* **ED-35,** 1510 (1988).
9. M. Kemp, MSc Thesis, Ecole Polytechnique de Montréal (1988).
10. D. L. Scharfetter and H. K. Gummel, *IEEE Trans. Electron Dev.* **ED-16,** 64 (1969).
11. E. H. Rhoderick, *Metal–Semiconductor Contacts*, Clarendon Press, Oxford (1980).
12. T. Yamamoto, M. Matsumoto and A. Yusa, *Solid-St. Electron.* **30,** 549 (1987).
13. C. Bulucea and A. Rusu, *Solid-St. Electron.* **30,** 1227 (1987).
14. J. Nishizawa and K. Yamamoto, *IEEE Trans. Electron Dev.* **ED-25,** 314 (1978).

APPENDIX A

Analytical Model for a 1-D a-Si:H Schottky Diode

Using the limiting cases of the SRH occupation function in the depleted and neutral regions[7] of a 1-D a-Si:H Schottky diode, Poisson's equation reads:

$$\frac{d^2\psi}{dx^2} = \begin{cases} \dfrac{-q}{\epsilon} g(E_f)(E_f - E_i^*) & 0 \leqslant x \leqslant x_0 \\ \dfrac{q^2}{\epsilon} g(E_f)\psi(x) & x_0 \leqslant x \leqslant d \end{cases} \quad \text{(A1)}$$

where $g(E_f)$ is the density of states at the Fermi level, $E_i^* = E_i - (kT/2)\log(\sigma_n/\sigma_p)$, x_0 is the position where $E_i^* = E_{fn}$ and where the Schottky contact is at $x = 0$ and the ohmic contact at $x = d$ (see Fig. 11). The solution to this equation is:

$$\psi(x) = \begin{cases} \psi(x=0) + A\dfrac{x}{\lambda} - \left(\dfrac{E_f - E_i^*}{2q}\right) \\ \qquad \times \dfrac{x^2}{\lambda^2} \quad 0 \leqslant x \leqslant x_0 \\ B\cosh\left(\dfrac{x}{\lambda}\right) + C\sinh\left(\dfrac{x}{\lambda}\right) \quad x_0 \leqslant x \leqslant d \end{cases} \quad \text{(A2)}$$

where $\lambda = \sqrt{\epsilon/q^2 g(E_f)}$. The boundary conditions appropriate to the finite length diode are[7]:

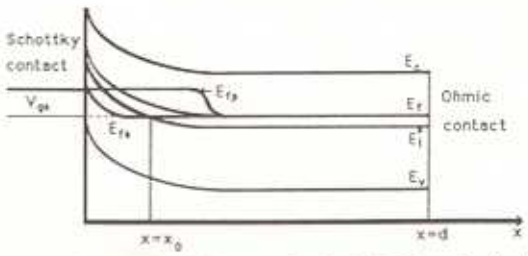

Fig. 11. Energy band diagram for the 1-D Schottky diode. The electrostatic potential is defined relative to E_f at the ohmic contact.

$$\begin{cases} \psi(x=0) = V_{gs} - \phi_B + \left(\dfrac{E_c - E_f}{q}\right) \\ \psi(x=d) = 0 \\ \psi(x=x_0) = -\left(\dfrac{E_f - E_i^*}{q}\right) \\ \dfrac{d\psi}{dx}(x = x_0 + \delta) = \dfrac{d\psi}{dx}(x = x_0 - \delta)\,\delta \to 0 \end{cases} \quad \text{(A3)}$$

where the two first conditions are self-explanatory, the third one can be understood by looking at Fig. 11 and the fourth is a continuity condition on the electric field. These conditions lead to the following equations:

$$\tanh\left(\frac{L - x_0}{\lambda}\right)\left[1 + \frac{q\psi(x=0)}{(E_f - E_i^*)} + \frac{1}{2}\left(\frac{x_0}{\lambda}\right)^2\right] + \left(\frac{x_0}{\lambda}\right) = 0 \quad \text{(A4)}$$

$$C = \frac{(E_f - E_i^*)}{q} \frac{\operatorname{sech}(x_0/\lambda)}{\tanh(d/\lambda) - \tanh(x_0/\lambda)} \quad \text{(A5)}$$

$$B = -C\tanh\left(\frac{d}{\lambda}\right) \quad \text{(A6)}$$

$$A = \left(\frac{\lambda}{x_0}\right)\left[\left(\frac{(E_f - E_i^*)}{2q}\right)\left[\left(\frac{x_0}{\lambda}\right)^2 - 2\right] - \psi(x-0)\right] \quad \text{(A7)}$$

Equation (A4) is a nonlinear equation in x_0 whose solution for a given value of V_{gs} enables one to calculate C, B and A and thus to obtain the electrostatic potential distribution between the gate and the source. An identical reasoning can be applied between the gate and the drain with the obvious substitution of V_{gs} by $V_{gs} - V_{ds}$ in eqn (A3). These equations are applied in conjunction with the diffusion model, eqn (22), to calculate the diode currents shown in Fig. 4.